

Quantum collision circuit, quantum invariants and quantum phase estimation procedure for fluid dynamic lattice gas automata

Niccolò Fonio^{a,b}, Pierre Sagaut^a, Giuseppe Di Molfetta^b

^a*M2P2, Aix-Marseille University, Central Marseille, M2P2 UMR 7340, 38 rue Joliot-Curie, Marseille, 13013, , France*

^b*LIS, Aix-Marseille university, LIS UMR 7020, Campus de Luminy, 163 avenue de Luminy, Marseille, 13288, , France*

Abstract

Lattice Gas Cellular Automata (LGCA) is a classical numerical method widely known and applied to simulate several physical phenomena. Among these phenomena, we find fluid flows described by the Navier-Stokes equations. We develop a quantum algorithm that allows for the simulation of fluid dynamic LGCA on a quantum computer. Furthermore, we prove the conservation of the quantities of interest, but finding more quantum invariants than expected. Finally, we develop a phase estimation procedure for detecting quantities of interest such as mass and momentum, avoiding reinitialization of the cell. In addition, we discuss a sublinear encoding of the lattice which admits a unitary streaming but constrains the collision step.

Keywords: Cellular Automata, Lattice gas, Quantum Computing, Quantum Circuits, Fluid-dynamic

1. Introduction

A *Lattice Gas Cellular Automata* (LGCA), addressed as DnQv model, is a gas of particles propagating in a discretized space of n dimensions where the components of the system (particles) can exhibit v discrete velocities [1]. Each LGCA consists of a lattice and a discrete evolution rule, made of a collision step when particles scatter in the lattice usually imposing some

Email address: `niccolo.fonio@lis-lab.fr` (Niccolò Fonio)

conservation laws, and a streaming step when particles move according to their velocity as shown in Figure 1.

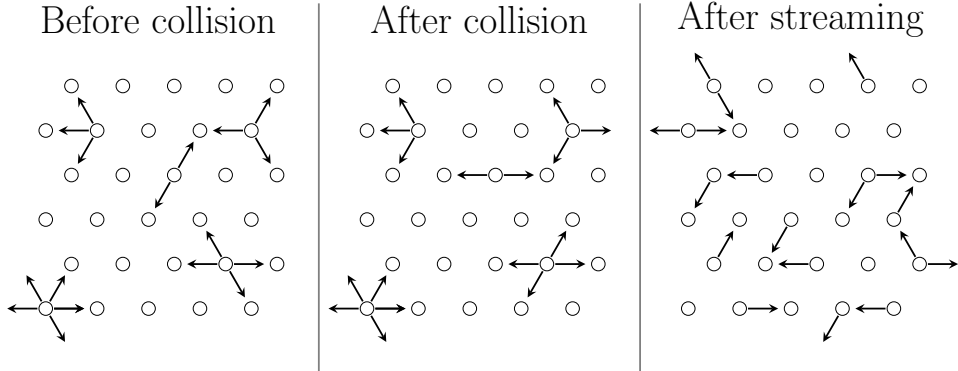


Figure 1: Evolution step for FHP. Before collision is the starting state of the lattice. In the center, we see that the particles in cells with the collisional states of Table.2 are rearranged. In the last part we see that particles have been streamed to neighboring cells applying periodic boundary conditions

This simple process is capable of simulating various physical phenomena. The fundamental concept behind LGCA is to have a microscopic system that preserves *exact* conservation laws with linear evolution. Then, at the macroscopic scale, it exhibits non-linear behavior, making it a good candidate for simulating Navier-Stokes equations and other non-linear phenomena. In this article, we deal with two LGCA, studying their quantum computing formulation. The first one is a one-dimensional model D1Q3, reported as a didactic example for the application of the methods here adopted. The second one is a 2D LGCA that was proved by Frisch, Hasslacher and Pomeau (FHP) to behave according to Navier-Stokes-like equations at the macroscopic level, thus demonstrating the potential of this numerical method.

Before giving the state of the art, it's worthy briefly addressing Lattice Boltzmann Methods (LBM). Starting from LGCA, the CFD community focused on lattice Boltzmann models (LBM), that are formally similar in the sense that they both rely on the combination of a streaming step with a collision step, but with the drastic difference that LBM is intrinsically non-linear (when simulating Navier-Stokes equations). They are based on streaming probability density functions instead of particles, solving the discrete Boltzmann equation. Both LGCA and LBM were proven to be successful in simulating several phenomena of interest, e.g. see [5, 6, 7, 8, 9, 10, 11, 12, 13,

14, 15, 17]. LGCA and LBM face the problem of scalability: the amount of computational resources needed scales linearly with the system size. Even if we can perform LGCA and LBM with today’s computers, we aim to open new perspectives by looking at the developing field of quantum computing for CFD [18, 19] to discover if it is possible to benefit from a quantum advantage, and we can explore the implications of using qubits instead of bits in LGCA.

This was the spirit of the first quantum models [20, 22, 23, 21, 24, 25], that focused on the physical character of the simulations, ending up in finite-difference methods or retrieving other physical equations as Dirac equation. These works used qubits to discretize the space and aimed to simulate their behavior for solving PDEs. The most recent development in this field regards Quantum LBM (QLBM) and consists of different approaches recently developed and in rapid expansion. One approach is to linearize the non-linear collision operator of LBM adopting Carleman linearization [26, 27]. Another one gets an exponential advantage in space complexity, requiring measurement at each time step [28, 29]. These first alternatives are probabilistic since they rely on a linear combination of unitaries [30, 31]. Alternative encodings and applications can be found, each with different advantages and drawbacks [33, 32].

While QLBM is intrinsically non-linear, imposing a step-by-step measurement and reinitialization, LGCA is intrinsically linear: the non-linearity arises from the complex behavior of the whole system. Thus, it is possible to map its evolution to the unitary evolution of a quantum algorithm. In this article, we develop a quantum algorithm for simulating the FHP LGCA on a quantum computer. We consider a linear encoding of the space, and we show how to implement efficiently 0-momentum collisions of the FHP model relying on two principal methodologies.

Accounting for the feature of measurement and reinitialization, we develop a quantum phase estimation (QPE) algorithm that allows to avoid them while being able to get information from the lattice state. Our method consists of moving the information to an additional smaller register, and we assess it with numerical simulations. We also prove that QPE can be used for practicing collision for the D1Q3 model. Then we show some unexpected results about conservation laws. Classically, the LGCA conserves some quantities of interest and some non-physical quantities, constraining the dynamics of the system. If we move to quantum computing, the definition of conserved quantities changes, since we consider observables, and so

does the definition of conservation. We can see that mass, momentum, and energy have quantum counterparts in the sum of Pauli gates [34].

We confirm that with a linear encoding of the space, these quantities are still conserved. However, they are not the only ones. With the method explained in the corresponding section, we also find the appearance of many additional quantum invariants in D1Q3 and FHP. The meaning of these quantities is out of the scope of the paper, and left as a future perspective.

In the appendix we show an alternative encoding with a sublinear encoding of the space. We show that streaming can be done with a quantum walk procedure, as shown in [28, 29], but we expand on the suggestion in [32] that streaming and collision cannot be done together at the same time with a sublinear number of qubits.

2. Methods

In this section, we consider a linear encoding of the space, requiring $O(Nv)$ qubits, where N is the number of cells and v is the number of velocities of the LGCA model. Using this encoding, we show different methodologies for deriving efficient implementation of collisional circuits, counting quantum invariants, and information retrieval through a quantum phase estimation algorithm. The encoding that we adopt is the Computational Basis Encoding (CBE) represented below:

$$\begin{aligned} \text{Classical encoding} &\longrightarrow \text{Quantum register} \\ \{n_v n_{v-1} \dots n_0\} &\longrightarrow |n_v n_{v-1} \dots n_0\rangle \end{aligned} \tag{1}$$

Instead of bits, we consider qubits, and instead of values 0 and 1 we consider the quantum states $|0\rangle$ and $|1\rangle$ for the absence and presence of a particle with respective velocity. We describe the state of the lattice with the following state

$$|\Psi\rangle = \bigotimes_{i=0}^N |\psi(i)\rangle = \bigotimes_{i=0}^N |n_v(i) \dots n_0(i)\rangle \tag{2}$$

where $|\psi(i)\rangle$ denotes the state of the i -th cell, and it corresponds to a register of v qubits. Regarding this encoding, the streaming procedure corresponds to a series of swap operations between qubits of different cells.

Introducing $\hat{S}(\vec{x}, v, \vec{x}', v')$ the swap operation between $|n_v(x)\rangle$ and $|n_{v'}(x')\rangle$, the streaming operation to be applied is

$$\hat{S} = \prod_x \prod_{\vec{v} \in V} \hat{S}(\vec{x}, \vec{v}, \vec{x}, -\vec{v}) \prod_x \prod_{\vec{v} \in V} \hat{S}(\vec{x}, \vec{v}, \vec{x} + \vec{v}, -\vec{v}) \quad (3)$$

where V is the set of positive (or negative) velocities. While D1Q3 has only deterministic collisions, FHP involves deterministic and non-deterministic collisions. The collision operator \hat{C} exchanges collisional states causing elastic collisions, and it depends on the DnQv model under consideration. For D1Q3 one circuit was proposed by love [34]. We propose an alternative collision circuit for D1Q3 that needs more qubits but shows an application for QPE to practice collisions. For FHP, to the best knowledge of the authors, an overall quantum circuit for performing deterministic and non-deterministic collision has not been proposed yet. The main difficulty is to leave all the non-collisional states unchanged. We propose two methods to implement a unique overall circuit performing 0-momentum collisions of FHP evolution. These methodologies can be further applied to other models or to other collisions.

2.1. Collisional quantum circuits

Using CBE we want to show two methods for finding collisional quantum circuits. The key idea is to use one or more ancillary qubits to be flipped if the cell is in a collisional configuration. Then, we apply a controlled collision with target the cell register, as shown in Figure 2.

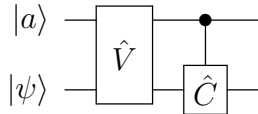


Figure 2: $|\psi\rangle$ is the cell register, $|a\rangle$ is the ancillary register, \hat{V} is the verification procedure, flipping the ancillary register only if there is a collisional state, \hat{C} is the controlled collision applied to the cell register

The first method is applied to D1Q3. Here we use two ancillary qubits for a QPE procedure with some specific operators, which identify a specific set of states. This is an example on how we can use QPE for the verification procedure.

The second method is applied to FHP. This involves the characteristics of the model to find optimal features to flip the conditional qubit. In fact, we are going to implement 2-, 3- and 4-body collisions through rotations of the cell, and the verification procedure is made with logical or equivalence class criteria. This gives an overall circuit for FHP, allowing for simulating FHP on a quantum computer.

For non-deterministic collisions, there are different options, and they depend on the model and the algorithm to be performed. In our CBE, non-determinism can be achieved with a superposition and a measurement. It is possible to create a superposition in the cell register directly. This is the favorable option if the algorithm retrieves information measuring directly the cell register. It is also possible to create a superposition with an ancillary qubit and then measure it instead of measuring the cell register. This is the methodology that will be applied for 2- and 4-body collisions in FHP.

2.2. Quantum invariants

We look at the conservation of local quantities as defined by Love [34], such as mass and momentum. Classically, for the discretization of the space, some nonphysical invariants arise [35]. The purpose of many studies has been to get rid of them for getting better results. Moolvig and Texeira made extensive work [4] for FCHC, which models a fluid in 3 dimensions. In our quantum computing framework we are able to calculate the exact number.

We define an observable \hat{O} as a *quantum invariant* if it commutes with the collision operator \hat{C} , so if it satisfies $[\hat{C}, \hat{O}] = 0$. We rewrite this property expanding the commutator as follows

$$\hat{C}\hat{O}\hat{C}^\dagger = \hat{O} \quad (4)$$

We can say that *any* operator \hat{O} respecting Eq.4 is a quantum invariant. If we want to know how many linearly independent quantum invariants there are for a QLGCA model, we apply the following procedure.

Consider a collision of a quantum DnQv model as a unitary operator \hat{C} . The number of linearly independent quantum invariants of a DnQv model is $l = 4^v - r$, where r is the rank of the evolution matrix M , with elements

$$M_{i,j} = \alpha_{i,j} - \delta_{i,j} \quad (5)$$

where

$$\hat{C}^\dagger \hat{O}_i \hat{C} = \sum_{j=0}^{4^v-1} \alpha_{i,j} \hat{O}_j$$

for $\hat{O}_i \in G_v$ where G_v is the Pauli Group with v qubits. This is proved by the fact that l corresponds to the number of linearly independent solutions of the linear system, where each equation is the conservation equation for the combination of Pauli gates on v qubits. This methodology is applied to D1Q3 and FHP, and confirms the expected conservation of mass and momentum operators, enlightening the existence of several more and unexpected quantum invariants.

2.3. Quantum Phase Estimation

Currently, recent proposals [28, 29] for Quantum LBM provide a measurement at each time step for retrieving information. We apply a phase estimation procedure to retrieve information about the state of the cell without measuring it directly. A similar methodology has been proposed [36]. We further consider explicit operators of physical value and application to efficient collision circuits. We move the desired information to an additional register $|q\rangle$ using a phase estimation algorithm, as shown in Figure 3.

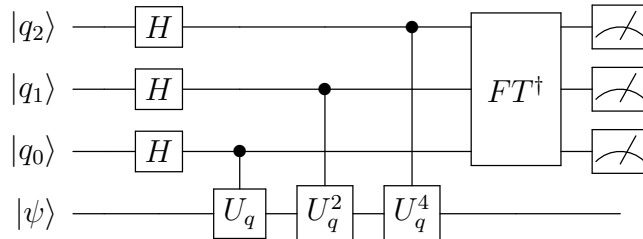


Figure 3: Phase estimation algorithm for mass detection. $ket\psi$ is the cell register, while $|q_2 q_1 q_0\rangle$ results in the binary value of the quantity detected. FT^\dagger corresponds to the inverse Fourier Transform

How to define quantum operators U in order to retrieve the information required such as mass or momentum? The purpose is to give to correspond each eigenvalue of U with the physical features of the cell. For example, all the states with the same mass have to be the same eigenvalue of the

mass operator \hat{U}_m . This can be achieved artificially defining the elements $U_q(s, s') = \delta_{s,s'} e^{iq(s)}$ for the cell quantity q . Alternatively, we can use specifically defined observables \hat{Q} , as mass and momentum given by Love, which give naturally the correct eigenvalues $\hat{U}_{\hat{Q}} = e^{i\hat{Q}}$.

3. Application to the D1Q3 model

3.1. The classical model

We consider D1Q3 as a didactic example. D1Q3 is a 1-dimensional lattice gas with a right-moving particle of mass 1, a left-moving particle of mass 1, and a rest particle of mass 2. Applying an exclusion principle, such that only one particle per velocity per site is allowed, each site is represented with a bit-string $[n_2 n_1 n_0]$. This system can simulate diffusion, but it is also the easiest model in which it is possible to perform collisions, ensuring mass and momentum conservation. An example of a 1-time step evolution of this gas is given in Figure 4. The collision allowed (and its inverse) consists of splitting a rest particle into two opposite-moving particles (the opposite is merging two opposite-moving particles into a rest particle).

x	0	1	2	3	4	5
Before collision	\circ	$\leftarrow \circ \rightarrow$	\bullet	$\circ \rightarrow \leftarrow \bullet$	\bullet	
	[000]	[101]	[010]	[001]	[110]	[010]
After collision	\circ	\bullet	$\leftarrow \circ \rightarrow$	$\circ \rightarrow \leftarrow \bullet$	$\leftarrow \circ \rightarrow$	
	[000]	[010]	[101]	[001]	[110]	[101]
After streaming	$\circ \rightarrow \leftarrow \bullet$	\circ	$\leftarrow \circ \rightarrow \leftarrow \bullet \rightarrow \circ$			
	[001]	[110]	[000]	[101]	[111]	[100]

Figure 4: D1Q3 evolution example. The presence of a rest particle is a black dot. The presence of a moving particle is an arrow. In this case, each cell is represented with 3 bits $[n_2 n_1 n_0]$. Before the collision in the cell at $x = 1, 2, 5$ there are collisional configurations, so they evolve according to the chosen collision. At $x = 4$ we do not have any collision for the exclusion principle. The streaming takes place according to respective velocity

As we can see, evolution is divided into collision and streaming. In the collision step the collisional states were rearranged. We note that this collision is deterministic, thus represented with a symmetric matrix that exchanges the two states $[010] \rightarrow [101]$, while leaving all the other states unchanged.

While classically we can write a pseudocode as reported for the collision step, to perform the same evolution on a quantum computer we give quantum gate-based circuit, interpreting operations as gates. The procedure for performing $|010\rangle \rightarrow |101\rangle$ has already been proposed by Love [34]. We try to validate an alternative, giving an example on how to use quantum phase estimation.

Algorithm 1 Collision D1Q3 algorithm

```

for cell  $\in$  lattice do
    if cell = [010] or cell = [101] then
        cell  $\leftarrow$  new state
    end if
end for

```

Classically, we can see that quantities such as mass $m(x) = \sum_i n_i(x)$ and momentum $p(x) = n_0(x) - n_1(x)$ are conserved. Averaging over neighbors we get mass density $\rho(x)$ and momentum density $\vec{u}(x)$. The behavior of these quantities in the continuum limit follows differential equations, which depend on the conservation laws applied.

3.2. Collision circuit

The collision operator matrix representation of D1Q3 is

$$\hat{C} = \begin{pmatrix} 1 & 0 & 0 & 0 & 0 & 0 & 0 & 0 \\ 0 & 1 & 0 & 0 & 0 & 0 & 0 & 0 \\ 0 & 0 & 0 & 0 & 0 & 1 & 0 & 0 \\ 0 & 0 & 0 & 1 & 0 & 0 & 0 & 0 \\ 0 & 0 & 0 & 0 & 1 & 0 & 0 & 0 \\ 0 & 0 & 1 & 0 & 0 & 0 & 0 & 0 \\ 0 & 0 & 0 & 0 & 0 & 0 & 1 & 0 \\ 0 & 0 & 0 & 0 & 0 & 0 & 0 & 1 \end{pmatrix} \quad (6)$$

A gate-based implementation of this is given in [34]. Even if Love's implementation is already optimal, we propose a didactic example on how to use specific operators for a QPE verification procedure. We start from the operators ZIZ and IZZ . If we look at their eigenvalues, practicing a QPE allows us to identify specific configurations. Dividing the space of possibilities again and again as shown in Figure 5, we arrive in the end to have a subset of the collisional state, $\{010, 101\}$ in our case.

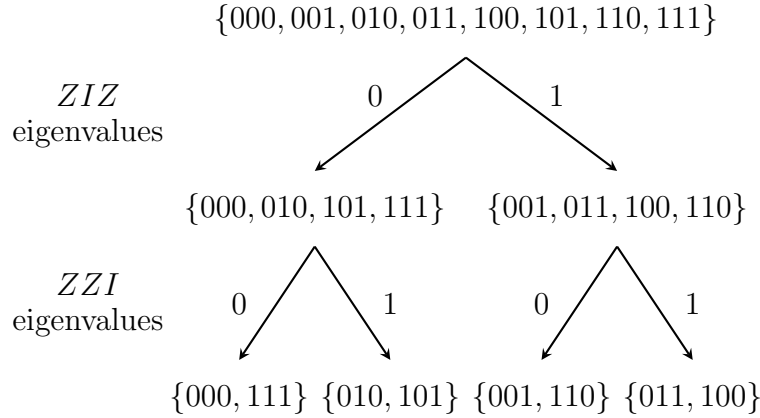


Figure 5: Tree scheme to see the partition of states depending on the detected eigenvalue of associated operator for QPE.

We can call *ZIZ* and *ZZI* the *discrimination operators*, and apply a QPE scheme as showed in Figure 6

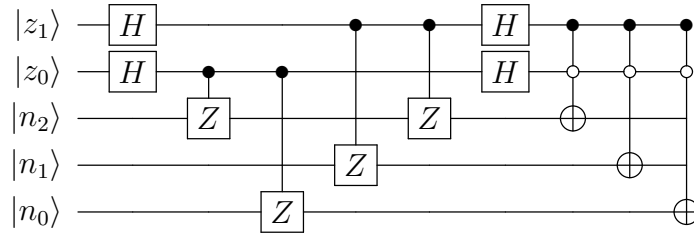


Figure 6: Alternative collision circuit for D1Q3. The first two qubits are conditional: the practicing of the collision, which is a series of Toffoli, depends on their state. This is a phase estimation algorithm with the first two as additional registers. The result, for the simplicity of the model, is deterministic.

3.3. Quantum invariants

The first thing to do for calculating the quantum invariants is writing the collision operator. The collision operator of D1Q3 presented in [34] can be written as

$$\hat{C}_{tot} = \frac{1}{4}(3III + IZZ + XXX + XYY - YXY + YYX - ZIZ + ZZI) \quad (7)$$

The second step is to calculate the evolution of each Pauli operator on 3 qubit space. The results are in Table B.5. From this it is possible to verify the conservation of mass m and momentum p as defined by Love :

$$m = IIZ + 2IZI + ZII \quad (8)$$

$$p = IIZ - ZII \quad (9)$$

Looking at all the evolved operators we see that there are more conserved quantities than expected. We can compute their number by calculating the evolution matrix and its rank. For D1Q3 the rank is equal to 14, meaning that there are 50 linearly independent conserved quantities.

Classical counterpart	Symmetric counterpart
III	XXX
IZZ, ZIZ, ZZI	XYY, YXY, YYX
$m = IIZ + 2IZI + ZII$	$XXY + 2YXX + YXX$
$p = IIZ - ZII$	$XXY - YXX$
	$IXI + XIX$

Table 1: We can see that the quantum formulation introduces a symmetry on conserved quantities. This happens also in FHP

The conservation of all these quantities is unexpected. The quantum invariants IZZ, ZIZ, ZZI have explainable classical counterparts as $n_0 \oplus n_1$, $n_0 \oplus n_2$, $n_1 \oplus n_2$. This has a clear explanation in the CBE adopted. The states $|0\rangle$ and $|1\rangle$ are the eigenstates of Z operator. Thus, the Z operator is reminiscent of the presence of a particle. Analysis of the physical meaning of all the other quantum invariants and hidden symmetries is out of the scope of the present paper and is left as a future perspective.

3.4. Quantum phase estimation for quantities

The methodology consists of defining the quantum operator to have the desired eigenvalues for a phase estimation procedure, as explained in the

methods section. For example, the matrix representation of the mass operator is the following

$$\hat{U}_m = \begin{pmatrix} 1 & 0 & 0 & 0 & 0 & 0 & 0 & 0 \\ 0 & e^{-i} & 0 & 0 & 0 & 0 & 0 & 0 \\ 0 & 0 & e^{-2i} & 0 & 0 & 0 & 0 & 0 \\ 0 & 0 & 0 & e^{-3i} & 0 & 0 & 0 & 0 \\ 0 & 0 & 0 & 0 & e^{-i} & 0 & 0 & 0 \\ 0 & 0 & 0 & 0 & 0 & e^{-2i} & 0 & 0 \\ 0 & 0 & 0 & 0 & 0 & 0 & e^{-3i} & 0 \\ 0 & 0 & 0 & 0 & 0 & 0 & 0 & e^{-4i} \end{pmatrix} \quad (10)$$

We clearly see that the eigenvalues of this operator correspond to $e^{-im(s)}$ where $m(s)$ is the mass of the state s (e.g. $m(\{001\}) = 1$). This turns the problem of measuring the mass of the cell into a phase estimation problem. Using U_m as an operator for QPE the circuit in Figure 3, we get the results in Figure 7. On the y-axis, we have the cell register and on the x-axis,

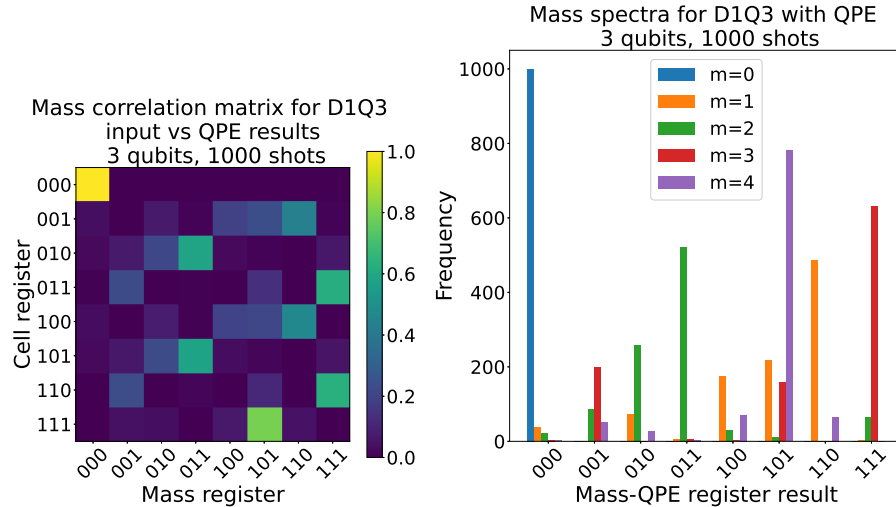


Figure 7: On the left: Outputs of the phase estimation algorithm in Figure 3 for each possible state obtained with 1000 shots. We can see the success of the QPE algorithm in identifying the same rows for states with the same quantities. On the right: output probability depending explicitly on the mass. We can distinguish different peaks that identify different masses with different outputs in the QPE register. The probabilities reported come from the states $\{000, 001, 101, 011, 111\}$

we have the mass register. We see that the rows of states $|001\rangle, |100\rangle$ and

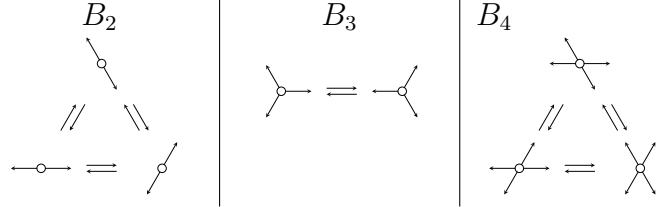


Table 2: These are the 0-momentum collisions of the model FHP model. We can notice that B_2 and B_4 are probabilistic rotations of 120° or 240° , taking place with equal probability, while B_3 is a rotation of 180° . B_2 and B_4 collisional states are invariant under B_3 , and vice versa

$|101\rangle, |010\rangle$, and $|110\rangle, |011\rangle$ are the same. This means that the algorithm is able to detect the same eigenvalues, i.e. the same mass. Analogous results for a major number of qubits and for momentum detection can be found with the same procedure, adapting the operator. A set of spectra improves with the distinguishability of the peaks of cells with different quantities.

4. Application to the FHP LGCA model

4.1. The classical model

The second LGCA we consider was proven by Frisch, Hasslacher, and Pomeau (FHP)[2] and Wolfram [3] to converge in the continuous limit to the Navier-Stokes equation. It is a 2-dimensional LGCA on a triangular lattice. The set of velocities $\{\vec{c}_i\}$ is defined as follows, and each c_i is linked to n_i and ordered as $[n_5 n_4 n_3 n_2 n_1 n_0]$

$$\vec{c}_i = \left(\cos\left(\frac{\pi}{3}i\right), \sin\left(\frac{\pi}{3}i\right) \right) \text{ for } i = 0, 1, \dots, 5 \quad (11)$$

Among different elastic collisions, we focus on 0-momentum collisions represented in Table 2. One evolution step is represented in Fig.1. A rest particle can be added for stability of the numerical simulations and for adding new collisions, causing a faster thermalization to the equilibrium of the solution. In this case, we can implement different collisions, but we first focus on 0-momentum collisions as represented in Table 2. If any cell in the lattice is found to be in a collisional state represented in Table 2, then a scattering process takes place and particles are rearranged. As explained, we can see these collisions as rotations, and rotations can also be applied to other invariant states, trivially the empty cell or the full cell, as we can see from Table 3

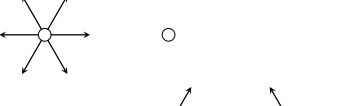
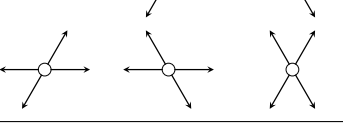
Invariant states	
B_2 collisional states	
B_4 collisional states	

Table 3: States with 0 asymmetric pairs. These states are invariant under a rotation of 180° , which corresponds to a B_3 collision.

Likewise the case of D1Q3, we show a quantum gate-based implementation for the collision step involving 0-momentum collisions.

The quantities that are conserved classically are, as before, mass $m(x) = \sum_{i=0}^5 n_i(x)$ and momentum $\vec{p}(x) = \sum_{i=0}^5 \vec{c}_i n_i(x)$. These quantities are averaged over neighbouring cells and their evolution is mapped to the continuous limit with a Chapman-Enskog expansion. This retrieves Euler's equations at the first order and Navier-Stokes equations at the second order [1]. We define the same quantities as quantum observables, verifying that they are conserved and we show how we can count the total amount of quantum invariants given a specific collision.

To know any quantity of the lattice gas, we need to recover the state of the lattice at each time step. While accessing memory in a classical computer is straightforward, in a quantum computer it relies on quantum measurements. If a quantum system is measured then it needs to be reinitialized generally. We give a quantum phase estimation procedure to avoid the measurement and reinitialization.

4.2. Collision circuit

We have v qubits at each site, these compose the *cell register*. Each collision is a rotation in the cell, as represented in Table 2. It is possible to define these rotations in terms of quantum operations, as a series of swaps gates Figure8.

Applying the method explained in the previous section, we develop an optimal overall circuit for the implementation of 0-momentum collisions in Table2, as shown in Figure 9. Each collision is implemented in two parts. We have the discrimination of the collisional states. It uses one conditional qubit $|b\rangle$, and the second part is the collision, which is a controlled operation

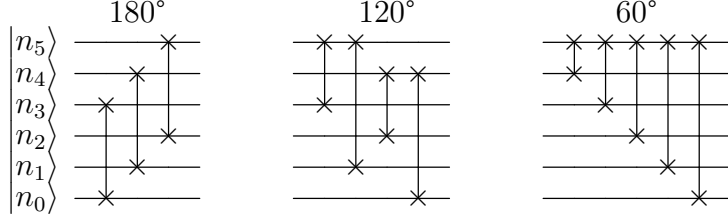


Figure 8: Rotations with quantum circuits

on the conditional qubit using an ancilla for simulating random outcomes of B_2 and B_4 .

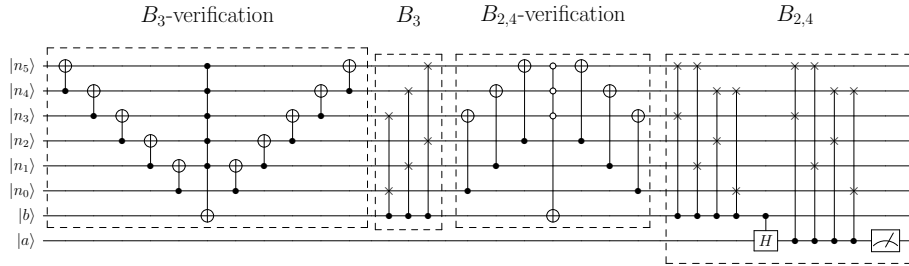


Figure 9: Collisional circuit for 0-momentum collisions of FHP. These are performed depending on a conditional qubit $|b\rangle$ that gets flipped if the input state is collisional, and an additional qubit $|a\rangle$ that introduces the non-deterministic character of 2- and 4-body collisions and is measured at each time-step. This circuit uses the invariance of collisional states for the merging of all the collisions in one circuit.

To implement the verification of collisional states of B_3 we consider a logic methodology, starting from the expression that can be found in [1], adapted to our convention.

$$b = (n_0 \wedge n_1) \& (n_1 \wedge n_2) \& (n_2 \wedge n_3) \& (n_3 \wedge n_4) \& (n_4 \wedge n_5) \quad (12)$$

Where \wedge is a XOR operation and $\&$ is an AND operation. We can turn this logic expression in a quantum circuit interpreting \wedge as CNOT and $\&$ as a generalized Toffoli gate with the cell's qubits as controls and $|b\rangle$ as a target. Then we restore the original cell and we apply the C-Swap gates for a rotation of 180° with $|b\rangle$ as a control qubit.

To implement B_2 and B_4 , we apply a reasoning based on equivalence classes. We define an *asymmetric opposite pair* as a pair of opposite bit-velocities that differ from each other (e.g. $|100000\rangle$ has 1 opposite pairs for the asymmetry between $|n_5\rangle$ and $|n_2\rangle$, $|110000\rangle$ has 2 asymmetric opposite pairs for $|n_5\rangle|n_4\rangle$ and $|n_2\rangle|n_1\rangle$, $|100100\rangle$ has 0 asymmetric opposite pairs). We consider the equivalence class of states with 0 asymmetric opposite pairs represented in Table3.

The collisional states of B_2 and B_4 belong to this class, and the other states are invariant under these collisions and under B_3 . Thus, we can target $|b\rangle$ to be $|1\rangle$ if there are no asymmetric opposite pairs. Then, with a series of C-Swaps with $|b\rangle$ as a control, we apply the first 120° rotation. To recall the non-deterministic character of the rule, we use a second ancilla $|a\rangle$ to create a superposition between different outcomes. We apply a controlled-H gate with $|b\rangle$ as control and $|a\rangle$, initialized to $|0\rangle$, as target. Then we apply the same controlled rotation of 120° with $|a\rangle$ as a control.

The circuit in Figure 9 was verified in qiskit applying a measurement on the cell register. The results are reported in Figure 10

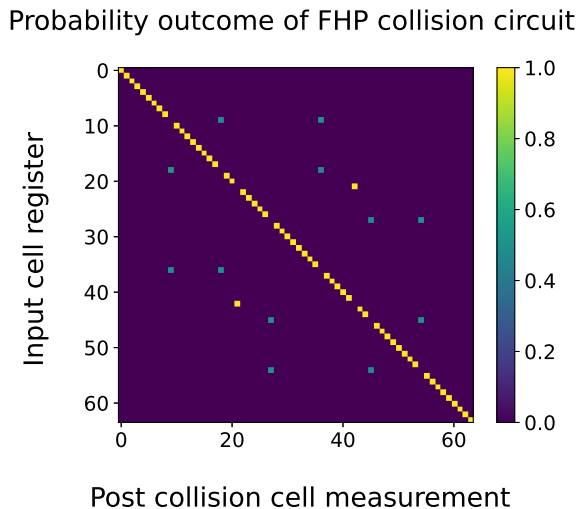


Figure 10: Probabilities of outcome from a measurement of the cell register at the end of the collisional circuit in Figure 9. We can see that the collision operator applied is a diagonal operator except for B_3 collisional states (21,42), B_2 collisional states (9,18,36), B_4 collisional states (27,45,54)

As a consequence, these non-deterministic rules create entangled qubits

within the cell. Superposition and entanglement are not physical features of a fluid dynamic simulation. Thus, a measurement of $|a\rangle$ can make the states collapse, exactly like a random extraction that takes place classically. Knowing the outcome of the collision is secondary to recovering the quantum state of the cell, thus it is not necessary to know it for retrieving the information needed. These two circuits can be merged for the invariance previously mentioned, as shown in Figure 9.

4.3. Quantum invariants

In the second place, we designed and applied the methodology of the evolution matrix M for finding the number of quantum invariants. For FHP we need first to introduce random collisions. For calculating the number of quantum invariants, we need to write the unitary operator \hat{C} . We cannot take it directly from Figure 9 because it involves ancillary qubits and applies a measurement, which makes the operator non-unitary. However, we can consider the analogous unitary operation that, instead of relying on an ancilla, creates a superposition of desired states. While for B_3 collisional states the procedure is standard and unitary, for $B_{2,4}$ we would need a superposition. We can consider B_2 as an example. We need an operator \hat{C} that practices the following operation

$$\hat{C} |a\rangle = \frac{|b\rangle + |c\rangle}{\sqrt{2}} \quad (13)$$

For $|a\rangle, |b\rangle, |c\rangle$ being different collisional states of B_2 or B_4 . This operator is non-unitary. Thus, we slightly modify the model to make it unitary, introducing the (low) possibility of no-collision. This can be done since no-collision operation does conserve mass and momentum. So we have

$$\hat{C} |a\rangle = \frac{-|a\rangle + 2|b\rangle + 2|c\rangle}{3} \quad (14)$$

This is a unitary operator and allows us to calculate the rank of the evolution matrix.

As we can see from Table 4 we verified that the number of quantum invariants becomes smaller if we increase the number of collisions. This was a result expected classically. Moreover, we verified the conservation of mass and momentum as the linear combination of Pauli operators defined by Love [34]

Collisions	Rank of M	Quantum invariants
B_3	126	3970
$B_{2,4}$	488	3608
$B_{2,3,4}$	590	3506

Table 4: Rank of evolution matrix corresponding to different collisions introduced in the unitary. The number of quantum invariants corresponds to $2^6 - r$ where r is the rank of the evolution matrix

$$M = Z_0 + Z_1 + Z_2 + Z_3 + Z_4 + Z_5 \quad (15)$$

$$P_x = Z_0 - Z_3 + \frac{1}{2}(Z_1 + Z_5 - Z_2 - Z_4) \quad (16)$$

$$P_y = \frac{\sqrt{3}}{2}(Z_1 + Z_2 - Z_4 - Z_5) \quad (17)$$

Where Z_i is the Z operator on the i -th qubit (e.g. $Z_2 = IIIZII$). Beyond these operators, analogously to D1Q3, other operators with a classical counterpart are conserved, considering $B_{2,3,4}$, as $I^{\otimes 6}$, Z_0Z_3 , Z_1Z_4 , $Z_0Z_1Z_3Z_4$ etc., as well as the symmetric respect to the $X^{\otimes 6}$ multiplication. All these quantities are unexpected, but we should consider that in the end we are emulating perfectly the classical system with its conservation laws. Thus, the resulting algorithm can be used for FHP simulation on a quantum computer. A more detailed analysis of the quantum invariants is out of the scope of this paper.

4.4. Quantum phase estimation for quantities

We applied the QPE procedure to FHP for mass and momentum in x and y directions. For each procedure we used the same operators as previously defined $U_q(s, s') = \delta_{s,s'} e^{iq(s)}$. The results we obtained are shown in Figure 11. Analogous simulations were run for momentum in x and y direction, analogously to D1Q3. The success of the algorithm can be qualitatively seen by the presence of one peak for each mass. We proved that a phase estimation algorithm offers an alternative to measuring directly the cell register, thus avoiding re-initialization of the system, which can keep evolving. This procedure can be equally applied to any DnQv model.

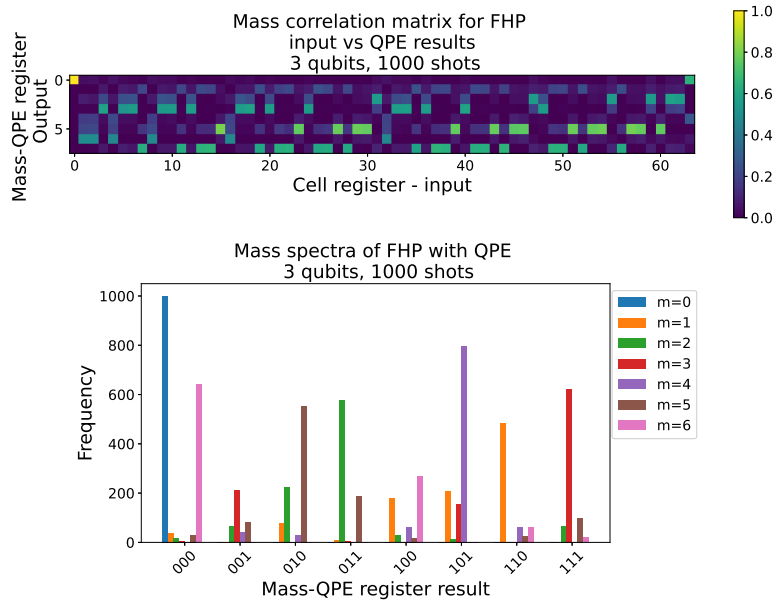


Figure 11: Above we find the correlation matrix: for each input state (x-axis) we plot the frequency of the result in the mass register (y-axis). Below we find the mass spectra barplot for different masses. These simulations are the result of the circuit in Figure 3

5. Conclusion

In this paper, we propose different ideas and methodologies for performing LGCA on a quantum computer. Considering $O(Nv)$ qubits for a DnQv model, we developed quantum algorithms for the FHP model, proving that it is possible to simulate this system on a quantum computer. To accomplish this, we developed two methodologies to be applied to finding other optimal circuits. We calculated the number of quantum invariants in D1Q3 and FHP, finding in both cases several more invariants than expected. The study of their role is yet to be investigated, as the eventual connection with classical invariants. We developed a phase estimation algorithm for detecting the quantities of the cell avoiding reinitialization of the cell register. The success of the QPE procedure is proven with numerical simulations.

Acknowledgments

This work is supported by the PEPR integrated project EPiQ ANR-22-PETQ-0007, by the ANR JCJC DisQC ANR-22-CE47-0002-01 founded from

the French National Research Agency and with the support of the french government under the France 2030 investment plan, as part of the Initiative d'Excellence d'Aix-Marseille Université - A*MIDEX AMX-21-RID-011.

Authors' contribution

Niccolo Fonio: conceptualization, data curation, methodology, formal analysis, investigation. **Giuseppe di Molfetta** and **Pierre Sagaut:** conceptualization, funding acquisition, writing - review & editing. All authors contributed to write, read and approved the final manuscript.

Declaration of competing interest

The author declare no competing interests

Appendix A. Sublinear encoding of the space

Observing the possibilities of a sublinear encoding of the space is of major interest for reducing drastically the number of qubits required, giving a practical advantage for these algorithms since they rely on large grids. Previous works [28, 29] have provided quantum algorithms for LBM simulations. Their remark is to practice the streaming step with a quantum walk procedure. We show that the same procedure applied to LGCA results in an exact evolution of the system, but constrains the collision step, as partly treated in [32]. We show, conversely to [32], that a unitary streaming is possible, but does not allow a collision step for the intrinsic indistinguishability of the cell imposed by the unitary streaming.

The most general sublinear encoding of the lattice is

$$|\Psi(t)\rangle = \frac{1}{\sqrt{N}} \sum_x |x\rangle |\psi(x, t)\rangle \quad (\text{A.1})$$

The information about the cell is contained in $|\psi(x)\rangle$. We can see that each cell needs to have some fundamental features. There must be information about each velocity and information about the occupation state of the corresponding velocity. The separability of velocities allows us to use a quantum walk procedure. The separability of the occupation state is necessary for the practicing of arbitrary collisions. One example is the following

encoding of the cell. The first register $|v\rangle$ represents the velocity, while the second qubit represents the occupation state

$$|\psi(x, t)\rangle = \frac{1}{\sqrt{V}} \sum_v |v\rangle |n_v(x, t)\rangle \quad (\text{A.2})$$

With this encoding, we have a correspondence between any classical state of the cell and the quantum counterpart, as we can see in this example of D1Q2 model, equal to D1Q3 without rest particle.

$$00 \longrightarrow |\psi_{00}\rangle = \frac{|00\rangle + |10\rangle}{\sqrt{2}} = |+0\rangle \quad (\text{A.3})$$

$$01 \longrightarrow |\psi_{01}\rangle = \frac{|00\rangle + |11\rangle}{\sqrt{2}} = |\beta_{00}\rangle \quad (\text{A.4})$$

$$10 \longrightarrow |\psi_{10}\rangle = \frac{|01\rangle + |10\rangle}{\sqrt{2}} = |\beta_{01}\rangle \quad (\text{A.5})$$

$$11 \longrightarrow |\psi_{11}\rangle = \frac{|01\rangle + |11\rangle}{\sqrt{2}} = |+1\rangle \quad (\text{A.6})$$

The direct advantage of this encoding is the streaming step, which can be translated in a series of controlled shift operators, implementing a quantum walk with the following operator

$$\hat{S} = \sum_v \hat{\Delta}_v \otimes |v\rangle \langle v| \otimes I = \sum_v \hat{\Delta}_v \otimes \hat{I}_v \quad (\text{A.7})$$

Where the identity acts on the occupation register because the streaming does not change the information about the occupation register, but only its location, and

$$\hat{\Delta}_v = \sum_x |x + v\rangle \langle x|$$

It is possible to prove, as shown later on, that the pre-streaming state and the after-streaming state for using \hat{S} are related as

$$|\psi(x, t + 1)\rangle = \sum_v \hat{I}_v |\psi(x - v, t)\rangle \quad (\text{A.8})$$

If we apply S to the lattice, in the cell-register we are going to have the subsystem of the cell that is divided depending on the velocity, according to the streaming operator.

$$\begin{aligned}
|\Psi(t+1)\rangle &= \hat{S} |\Psi(t)\rangle \\
&= \left(\sum_v \hat{\Delta}_v \otimes \hat{I}_v \right) \frac{1}{\sqrt{N}} \sum_x |x\rangle |\psi(x, t)\rangle \\
&= \frac{1}{\sqrt{N}} \sum_x \sum_v \hat{\Delta}_v |x\rangle \otimes \hat{I}_v |\psi(x, t)\rangle \\
&= \frac{1}{\sqrt{N}} \sum_x \sum_v |x+v\rangle \otimes \hat{I}_v |\psi(x, t)\rangle
\end{aligned}$$

If we expand this sum in the case of D1Q2, we have 2 velocities $v \in \{-1, 1\}$.

$$\begin{aligned}
|\Psi(t+1)\rangle &= \frac{1}{\sqrt{N}} \sum_{x=1}^N \sum_v |x+v\rangle \otimes \hat{I}_v |\psi(x, t)\rangle \\
&= |N\rangle \otimes \hat{I}_{-1} |\psi(1, t)\rangle + |2\rangle \otimes \hat{I}_1 |\psi(1, t)\rangle + \quad (A.9) \\
&\quad + |1\rangle \otimes \hat{I}_{-1} |\psi(2, t)\rangle + |3\rangle \otimes \hat{I}_1 |\psi(2, t)\rangle + \\
&\quad + |2\rangle \otimes \hat{I}_{-1} |\psi(3, t)\rangle + |4\rangle \otimes \hat{I}_1 |\psi(3, t)\rangle + \dots
\end{aligned}$$

Then, we can rewrite this sum as follows

$$|\Psi(t+1)\rangle = \sum_x |x\rangle \otimes \left[\hat{I}_1 |\psi(x-1, t)\rangle + \hat{I}_{-1} |\psi(x+1, t)\rangle \right] \quad (A.10)$$

In general, we can write

$$\begin{aligned}
|\Psi(t+1)\rangle &= \sum_x |x\rangle \otimes \sum_v \hat{I}_v |\psi(x-v, t)\rangle \\
&= \sum_x |x\rangle \otimes |\psi(x, t+1)\rangle
\end{aligned}$$

Where

$$|\psi(x, t+1)\rangle = \sum_v \hat{I}_v |\psi(x-v, t)\rangle \quad (A.11)$$

The Eq.A.8 depends directly on the choice of performing a quantum walk for moving the information through the lattice. It says that the information after the streaming (lhs) merges information before the streaming (rhs). The

streaming procedure is represented in Fig.A.12, with the algorithm that consists of an initialization procedure and the streaming operators. These can be implemented with various methods [37, 38, 39]. Results of this algorithm are shown in A.13

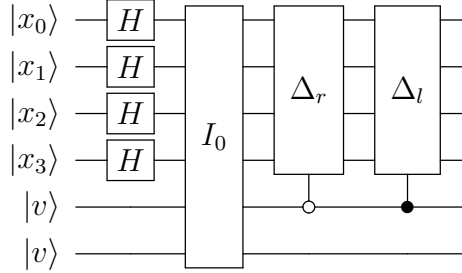


Figure A.12: Quantum circuit with unitary steaming for D1Q2. The x register is the space register, v is the velocity register and n is the occupation register. Here we count $2^4 = 16$ sites. The I_0 operation is a series of generalized Toffoli that initialize the occupation qubits in the n register. The controlled Δ_v operations are repeated for each time step

The states of the proposed example are not orthogonal. Thus, an arbitrary collision cannot be performed. Is there an alternative to Eq.A.2 that ensures orthogonality preserving the same streaming operator? To answer, we define the most general states as follows, in matrix notation for simplicity, we consider a cell register of 2 qubits

$$|\psi_{i,j}\rangle = \begin{bmatrix} a_{i,j} \\ b_{i,j} \\ c_{i,j} \\ d_{i,j} \end{bmatrix} \quad (\text{A.12})$$

Using $|v_0\rangle = |0\rangle$, $|v_1\rangle = |1\rangle$ and we try to solve Eq.A.8. We can formulate Eq.A.8 for D1Q2 as follows $\forall k, k' \in 0, 1, 2, 3$

$$|\psi_{ij}\rangle = I_0 |\psi_{ik}\rangle + I_1 |\psi_{k'j}\rangle \quad (\text{A.13})$$

This is a set of 16 equations. Some of them are trivial and if we generally use Eq.A.12, we find that there are 8 conditions to respect

$$\begin{array}{llll} c_{00} = c_{10} & d_{00} = d_{10} & a_{00} = a_{01} & b_{00} = b_{01} \\ c_{11} = c_{01} & d_{11} = d_{01} & a_{11} = a_{10} & b_{11} = b_{10} \end{array} \quad (\text{A.14})$$

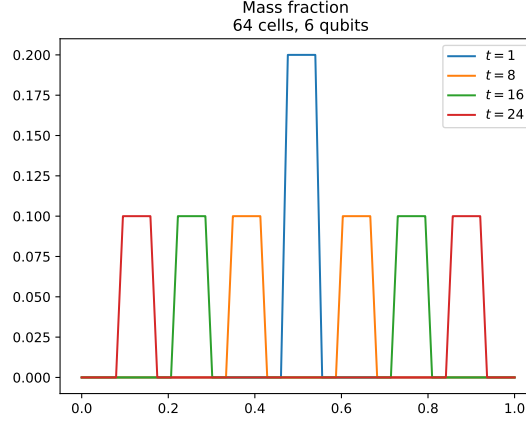


Figure A.13: D1Q2 lattice at different time-steps with 64 cells run with the quantum circuit in Fig.A.12. This simulation was run with mps simulator by Qiskit. At increasing time steps we can see the system diffuses and particles move according to respective velocities. After each value of t the system was measured 1000 shots.

We can rewrite our states as follows

$$\begin{aligned}
 |\psi_{00}\rangle &= \begin{pmatrix} a \\ b \\ c \\ d \end{pmatrix} & |\psi_{01}\rangle &= \begin{pmatrix} a \\ b \\ e \\ f \end{pmatrix} \\
 |\psi_{10}\rangle &= \begin{pmatrix} g \\ h \\ c \\ d \end{pmatrix} & |\psi_{11}\rangle &= \begin{pmatrix} g \\ h \\ e \\ f \end{pmatrix}
 \end{aligned}$$

Now we can apply the orthogonality condition and we get these 6 equations

$$\langle \psi_{i,j} | \psi_{i',j'} \rangle = \delta_{i,i'} \delta_{j,j'} \quad (\text{A.15})$$

We apply the following definitions to rewrite A.15

$$\begin{aligned}
A &= |a|^2 + |b|^2 \\
B &= |c|^2 + |d|^2 \\
C &= |e|^2 + |f|^2 \\
D &= |g|^2 + |h|^2 \\
E &= a^*g + b^*h \\
F &= c^*e + d^*f
\end{aligned}$$

And we get the following set of equations

$$\begin{array}{llll}
A + F = 0 & E + B = 0 & E + F = 0 & E + F^* = 0 \\
E + C = 0 & D + F = 0 & A + B = 1 & A + C = 1 \\
B + D = 1 & & C + D = 1 &
\end{array}$$

It is easy now to see that these equations are not solvable, since according to the first two $A+B = 0$, while the normalization condition imposes $A+B = 1$. The peculiar aspect is that even increasing the space, i.e. increasing the qubits for an encoding, brings to the same set of equations. We believe that they are intrinsically caused by the streaming operator separating the information, making it impossible to merge it in a distinguishable way. These considerations are intended as a hint that a sublinear encoding preserving orthogonality in the cell register and performing the evolution of LGCA through quantum walk is not possible.

In conclusion, this encoding does not permit the practice of the collision step, for the impossibility of ensuring the orthogonality of the cell states. Our result is restricted to the case of the chosen velocities $|0\rangle$ and $|1\rangle$, and of the streaming operator Eq.A.7. A general proof for this impossibility is yet to be found. Alternative streaming would change the character of the algorithm, which is conceived as a naive translation of the classical algorithm using a superposition.

Appendix B. Complete evolution of D1Q3 operators

In this table we give all the evolved operators as calculated with the collision provided by Love. Thus, it is possible to verify directly the conservation of the quantities reported in the article. Analogous evolved operator for FHP can be provided upon request

Input state \hat{O}	Output state $\hat{C}^\dagger \hat{O} \hat{C}$	Input state \hat{O}	Output state $\hat{C}^\dagger \hat{O} \hat{C}$
III	III	XZZ	$\frac{1}{2}(-IXX - IYY + XII + XZZ)$
IIX	$\frac{1}{2}(IIX + XXI + YYI + ZZX)$	YII	$\frac{1}{2}(-IXY + IYX + YII + YZZ)$
IYI	$\frac{1}{2}(IYI + XYI - YXI + ZZY)$	YIX	$\frac{1}{2}(IYI - XIY + YIX + ZYZ)$
IIZ	$\frac{1}{2}(IIZ + IZI - ZII + ZZZ)$	YIY	$\frac{1}{2}(-IXI + XIX + YIY - ZXZ)$
IXI	$\frac{1}{2}(IXI + XIX - YIY - ZXZ)$	YIZ	$\frac{1}{2}(YIZ + YZI + ZXY - ZYX)$
IXX	$\frac{1}{2}(IXX - IYY + XII - XZZ)$	YXI	$\frac{1}{2}(-IYY + XYI + YXI + ZZY)$
IXY	$\frac{1}{2}(IXY + IYX - YII + YZZ)$	YXX	$\frac{1}{2}(-XXY + XYX + YXX - YYY)$
IXZ	$\frac{1}{2}(IXZ + XZX - YZY - ZXI)$	YXY	YXY
IYI	$\frac{1}{2}(IYI + XIY + YIX - ZYZ)$	YXZ	$\frac{1}{2}(-IZY + XYZ + YXZ + ZIY)$
IYX	$\frac{1}{2}(IYX + IYX + YII - YZZ)$	YYI	$\frac{1}{2}(IIX - XXI + YYI - ZZX)$
IYY	$\frac{1}{2}(-IXX + IYY + XII - XZZ)$	YYX	YYX
IYZ	$\frac{1}{2}(IYZ + XZY + YZX - ZYI)$	YYY	$\frac{1}{2}(-XXY + XYX - YXX + YYY)$
IZI	$\frac{1}{2}(IIZ + IZI + ZII - ZZZ)$	YYZ	$\frac{1}{2}(IZX - XXZ + YYZ - ZIX)$
IZX	$\frac{1}{2}(IZX + XXX + YYZ + ZIX)$	YZI	$\frac{1}{2}(YIZ + YZI - ZXY + ZYX)$
IZY	$\frac{1}{2}(IZY + XYZ - YXZ + ZIY)$	YZX	$\frac{1}{2}(IYZ - XZY + YZX + ZYI)$
IZZ	IZZ	YZY	$\frac{1}{2}(-IXZ + XZX + YZY - ZXI)$
XII	$\frac{1}{2}(IXX + IYY + XII + XZZ)$	YZZ	$\frac{1}{2}(IYX - IYX + YII + YZZ)$
XIX	$\frac{1}{2}(IXI + XIX + YIY + ZXZ)$	ZII	$\frac{1}{2}(-IIZ + IZI + ZII + ZZZ)$
XIY	$\frac{1}{2}(IYI + XIY - YIX + ZYZ)$	ZIX	$\frac{1}{2}(IZX - XXZ - YYZ + ZIX)$
XIZ	$\frac{1}{2}(XIZ + XZI - ZXX - ZYY)$	ZIY	$\frac{1}{2}(IYZ - XYZ + YXZ + ZIY)$
XXI	$\frac{1}{2}(IIX + XXI - YYI - ZZX)$	ZIZ	ZIZ
XXX	XXX	ZXI	$\frac{1}{2}(-IXZ + XZX - YZY + ZXI)$
XXY	$\frac{1}{2}(XXY + XYX - YXX - YYY)$	ZXX	$\frac{1}{2}(-XIZ + XZI + ZXX - ZYY)$
XXZ	$\frac{1}{2}(IZX + XXX - YYZ - ZIX)$	ZXY	$\frac{1}{2}(YIZ - YZI + ZXY + ZYX)$
XYI	$\frac{1}{2}(IYI + XYI + YXI - ZZY)$	ZXZ	$\frac{1}{2}(-IXI + XIX - YIY + ZXZ)$
XYX	$\frac{1}{2}(XXY + XYX + YXX + YYY)$	ZYI	$\frac{1}{2}(-IYZ + XZY + YZX + ZYI)$
XYY	XYY	ZYX	$\frac{1}{2}(-YIZ + YZI + ZXY + ZYX)$
XYZ	$\frac{1}{2}(IYZ + XYZ + YXZ - ZIY)$	ZYY	$\frac{1}{2}(-XIZ + XZI - ZXX + ZYY)$
XZI	$\frac{1}{2}(XIZ + XZI + ZXX + ZYY)$	ZYZ	$\frac{1}{2}(-IYI + XIY + YIX + ZYZ)$
XZX	$\frac{1}{2}(IXZ + XZX + YYZ + ZXI)$	ZZI	ZZI
XZY	$\frac{1}{2}(IYZ + XZY - YZX + ZYI)$	ZZX	$\frac{1}{2}(IIX - XXI - YYI + ZZX)$
XZZ	$\frac{1}{2}(-IXX - IYY + XII + XZZ)$	ZZY	$\frac{1}{2}(IYI - XYI + YXI + ZZY)$

Table B.5: Table of the evolution of all the D1Q3 Pauli operators

References

- [1] Wolf-Gladrow, D. Lattice-gas cellular automata and lattice Boltzmann models: an introduction. (Springer,2004)
- [2] Frisch, U., Hasslacher, B. & Pomeau, Y. Lattice-gas automata for the Navier-Stokes equation. *Physical Review Letters*. **56**, 1505 (1986)
- [3] Wolfram, S. Cellular automaton fluids 1: Basic theory. *Journal Of Statistical Physics*. **45** pp. 471-526 (1986)
- [4] Molvig, K., Donis, P., Miller, R., Myczkowski, J. & Vichniac, G. Multi-

species lattice-gas automata for realistic fluid dynamics. *Cellular Automata And Modeling Of Complex Physical Systems: Proceedings Of The Winter School, Les Houches, France, February 21-28, 1989.* pp. 206-231 (1989)

- [5] Mainster, M. Cellular automata: retinal cells, circulation and patterns. *Eye.* **6**, 420-427 (1992)
- [6] F Brandner, A., Timr, S., Melchionna, S., Derreumaux, P., Baaden, M. & Sterpone, F. Modelling lipid systems in fluid with Lattice Boltzmann Molecular Dynamics simulations and hydrodynamics. *Scientific Reports.* **9**, 1-14 (2019)
- [7] McCullough, J. & Coveney, P. An efficient, localised approach for the simulation of elastic blood vessels using the lattice Boltzmann method. *Scientific Reports.* **11**, 24260 (2021)
- [8] Nava-Sedeño, J., Hatzikirou, H., Klages, R. & Deutsch, A. Cellular automaton models for time-correlated random walks: derivation and analysis. *Scientific Reports.* **7**, 16952 (2017)
- [9] Roy, I., Ray, P. & Balasubramanian, G. Examining oxidation in β -NiAl and β -NiAl+ Hf alloys by stochastic cellular automata simulations. *Npj Materials Degradation.* **5**, 55 (2021)
- [10] Stockman, H., Stockmant, C. & Carrigan, C. Modelling viscous segregation in immiscible fluids using lattice-gas automata. *Nature.* **348** pp. 523-525 (1990)
- [11] Appert, C., Rothman, D. & Zaleski, S. A liquid-gas model on a lattice. *Physica D: Nonlinear Phenomena.* **47**, 85-96 (1991)
- [12] Chopard, B. & Droz, M. Cellular automata model for heat conduction in a fluid. *Physics Letters A.* **126**, 476-480 (1988)
- [13] Frenkel, D. & Ernst, M. Simulation of diffusion in a two-dimensional lattice-gas cellular automaton: a test of mode-coupling theory. *Physical Review Letters.* **63**, 2165 (1989)
- [14] Simons, N., Bridges, G., Podaima, B. & Sebak, A. Cellular automata as an environment for simulating electromagnetic phenomena. *IEEE Microwave And Guided Wave Letters.* **4**, 247-249 (1994)

- [15] Chen, S., Chen, H., Martnez, D. & Matthaeus, W. Lattice Boltzmann model for simulation of magnetohydrodynamics. *Physical Review Letters*. **67**, 3776 (1991)
- [16] Chen, S. & Doolen, G. Lattice Boltzmann method for fluid flows. *Annual Review Of Fluid Mechanics*. **30**, 329-364 (1998)
- [17] Boghosian, B. & Levermore, C. A cellular automaton for Burgers' equation. *Complex Systems*. **1**, 17-30 (1987)
- [18] Bharadwaj, S. & Sreenivasan, K. Quantum computation of fluid dynamics. *ArXiv Preprint arXiv:2007.09147*. (2020)
- [19] Succi, S., Itani, W., Sreenivasan, K. & Steijl, R. Quantum computing for fluids: Where do we stand?. *Europhysics Letters*. **144**, 10001 (2023)
- [20] Yepez, J. Quantum lattice-gas model for computational fluid dynamics. *Physical Review E*. **63**, 046702 (2001)
- [21] Yepez, J. Quantum lattice-gas model for the Burgers equation. *Journal Of Statistical Physics*. **107** pp. 203-224 (2002)
- [22] Yepez, J. Quantum lattice-gas model for the diffusion equation. *International Journal Of Modern Physics C*. **12**, 1285-1303 (2001)
- [23] Yepez, J. & Boghosian, B. An efficient and accurate quantum lattice-gas model for the many-body Schrödinger wave equation. *Computer Physics Communications*. **146**, 280-294 (2002)
- [24] Meyer, D. Quantum lattice gases and their invariants. *International Journal Of Modern Physics C*. **8**, 717-735 (1997)
- [25] Meyer, D. Quantum mechanics of lattice gas automata: One-particle plane waves and potentials. *Physical Review E*. **55**, 5261 (1997)
- [26] Itani, W., Sreenivasan, K. & Succi, S. Quantum algorithm for lattice Boltzmann (QALB) simulation of incompressible fluids with a nonlinear collision term. *Physics Of Fluids*. **36** (2024)
- [27] Itani, W. & Succi, S. Analysis of Carleman Linearization of Lattice Boltzmann. *Fluids*. **7**, 24 (2022)

- [28] Budinski, L. Quantum algorithm for the advection–diffusion equation simulated with the lattice Boltzmann method. *Quantum Information Processing*. **20**, 57 (2021)
- [29] Budinski, L. Quantum algorithm for the Navier Stokes equations by using the streamfunction vorticity formulation and the lattice Boltzmann method. *ArXiv Preprint arXiv:2103.03804*. (2021)
- [30] Childs, A. & Wiebe, N. Hamiltonian simulation using linear combinations of unitary operations. *ArXiv Preprint arXiv:1202.5822*. (2012)
- [31] Low, G. & Chuang, I. Hamiltonian simulation by qubitization. *Quantum*. **3** pp. 163 (2019)
- [32] Schalkers, M. & Möller, M. On the importance of data encoding in quantum Boltzmann methods. *Quantum Information Processing*. **23**, 20 (2024)
- [33] Todorova, B. & Steijl, R. Quantum algorithm for the collisionless Boltzmann equation. *Journal Of Computational Physics*. **409** pp. 109347 (2020)
- [34] Love, P. On quantum extensions of hydrodynamic lattice gas automata. *Condensed Matter*. **4**, 48 (2019)
- [35] Bernardin, D. Global invariants and equilibrium states in lattice gases. *Journal Of Statistical Physics*. **68** pp. 457-495 (1992)
- [36] Chrit, F., Kocherla, S., Gard, B., Dumitrescu, E., Alexeev, A. & Bryngelson, S. Fully quantum algorithm for lattice Boltzmann methods with application to partial differential equations. *ArXiv Preprint arXiv:2305.07148*. (2023)
- [37] Wing-Bocanegra, A. & Venegas-Andraca, S. Circuit implementation of discrete-time quantum walks via the shunt decomposition method. *Quantum Information Processing*. **22**, 146 (2023)
- [38] Shakeel, A. Efficient and scalable quantum walk algorithms via the quantum Fourier transform. *Quantum Information Processing*. **19**, 323 (2020)

- [39] Razzoli, L., Cenedese, G., Bondani, M. & Benenti, G. Efficient implementation of discrete-time quantum walks in NISQ devices. *ArXiv Preprint arXiv:2402.01854*. (2024)
- [40] Schumacher, B. & Werner, R. Reversible quantum cellular automata. *ArXiv Preprint quant-ph/0405174*. (2004)